Scanning Tunneling Microscopic Study with Atomic Resolution of the Dissolution of Cu(111) in Aqueous Chloride Solutions

D. Wayne Suggs and Allen J. Bard*

Contribution from the Department of Chemistry and Biochemistry, The University of Texas at Austin, Austin, Texas 78712

Received February 24, 1994. Revised Manuscript Received July 1, 1994[⊗]

Abstract: In situ scanning tunneling microscopy (STM) of the dissolution of a Cu(111) electrode in aqueous chloride media (HCl and KCl) was employed to ascertain the mechanism of the reaction at the atomic level. At potentials where there was no dissolution, atomic imaging of the Cu(111) revealed a $(6\sqrt{3}\times6\sqrt{3})R30°$ structure consisting of a Cl adlattice with a Cl–Cl distance of 0.39 ± 0.02 nm which is in agreement with vacuum surface analytical (low-energy electron diffraction, Auger electron analysis and STM) studies of Cu(111) dosed with chlorine and aqueous Cl^-. Imaging at potentials where the anodic dissolution of Cu begins reveals that the preferred reaction sites were step edges, and the retreating edges always ran along steps in the {211} direction. Rates of dissolution increased as the potential was increased, with the predominant reaction site being step edges. The dissolution rate was higher in the presence of K^+.

Introduction

Metal electrochemical surface processes, i.e., dissolution, corrosion, and electrodeposition in aqueous electrolytes, have been studied for many years because of their practical importance and theoretical interest.[1] Until recently, most studies to elucidate the mechanisms of these processes were electrochemical ones, e.g., voltammetric measurements, where thermodynamic and kinetic parameters were obtained by comparing experimental results to proposed models. These studies have been useful in providing a macroscopic picture of these processes, but clearly cannot provide a microscopic (atomic level) understanding.

A view of these processes at the atomic level is important to elucidate the role of defects and step edges in the dissolution process that can affect corrosion,[2] adsorption,[3] catalysis,[4] and interfacial chemistry.[5] Optical and electron microscopic investigations have been the usual methods used to study dissolution reactions, e.g., where the surface is chemically etched to reveal dislocation positions. The etched surface usually shows the presence of micrometer-sized pits. However, these methods cannot distinguish whether the pits grew from a single atomic defect or from surface diffusion of vacancies. An important disadvantage of these techniques is that the surface cannot be monitored in situ to reveal the mechanism of dissolution with atomic-scale resolution.

In recent times, the scanning tunneling microscope (STM)[6] and the atomic force microscope (AFM)[7] have been applied to the atomic imaging of surface features of electrodes, both ex situ[8a,b] and in situ.[7b,8c–h] For example, in situ imaging of structures formed during electrodeposition[7b,8e,f] surface reconstruction[8g] or by oxidation–reduction cycles[8h] has been carried out with an electrode under potential control (electrochemical STM and AFM). The scanning tunneling microscope can be used to observe, in real time, processes such as dealloying,[9] corrosion of metals,[10] and surface reordering.[8h,11] The results of these investigations have provided useful insight toward understanding diffusion and dissolution mechanisms at the atomic level. Among the questions of interest in such studies are the relative rates of etching reactions at defect sites, kinks, and step edges compared to those on terraces, the effects of surface diffusion, and the importance of specific adsorption, e.g., of solution anions, on these processes.

Many STM studies have employed noble metal electrodes (e.g., Au or Au alloys) or C. However, more active metals are clearly of interest. We have chosen to study the Cu/aqueous solution interface and the etching of Cu by STM. Cu etching and corrosion are of interest in the electronics industry, e.g., in printed circuit boards. Moreover, although more active than the noble metals, Cu is one of the more stable metals because of its high hydrogen overpotential and the absence of surface oxide in acidic solutions.[12] Several electrochemical studies of

[⊗] Abstract published in *Advance ACS Abstracts,* October 15, 1994.

(1) *Corrosion Mechanisms*; Mansfeld, F., Ed.; Marcel Dekker: New York, 1987.

(2) Sieradski, K.; Corderman, R. R.; Shukla, D.; Neuman, R. C. *Philos. Mag. A* **1989**, *59*, 713.

(3) Hubbard, A. T. *Chem. Rev.* **1988**, *88*, 633.

(4) Dubois, L. H.; Hansma, P. K.; Somorjai, G. A. *Appl. Surf. Sci.* **1990**, *6*, 173.

(5) Sangwal, K. In *Etching of Crystals: Theory, Experiment, and Applications*; Amelinckx, S., Nihoul, J., Eds.; North-Holland: Amsterdam, 1987.

(6) (a) Binning, G.; Rohrer, H. *IBM J. Res. Dev.* **1986**, *30*, 355. (b) *Scanning Tunnelling Microscopy and Related Methods*; Behm, R. J., Garcia, N., Rohrer, H., Eds.; NATO ASI Series; Kluwer: The Netherlands, 1990; Vol. 184.

(7) (a) Manne, S.; Butt, H.-J.; Gould, S. A. C.; Hansma, P. K. *Appl. Phys. Lett.* **1990**, *56*, 1758. (b) Chen, C. H.; Gewirth, A. A. *J. Am. Chem. Soc.* **1992**, *114*, 5439.

(8) (a) Schardt, B. C.; Yau, S. L.; Rinaldi, F. *Science* **1989**, *243*, 1050. (b) Haiss, W.; Sass, J. K.; Gao, X.; Weaver, M. J. *Surf. Sci. Lett.* **1992**, *274*, L593. (c) Yau, S. L.; Vitrus, C. M.; Schardt, B. C. *J. Am. Chem. Soc.* **1990**, *112*, 3677. (d) Gao, X.; Weaver, M. J. *J. Am. Chem. Soc.* **1992**, *114*, 8544. (e) Batina, N.; Will, T.; Kolb, D. M. *Faraday Discuss.* **1992**, *94*, 1. (f) Hendricks, S. A.; Kim, Y. T.; Bard, A. J. *J. Electrochem. Soc.* **1992**, *139*, 2818. (g) Gao, X.; Hamelin, A.; Weaver, M. *J. Phys. Rev. Lett.* **1991**, *67*, 618. (h) Trevor, D. J.; Chidsey, C. E. D.; Loiacono, D. N. *Phys. Rev. Lett.* **1989**, *62*, 929.

(9) (a) Moffat, T.; Fan, F.-R. F.; Bard, A. J. *J. Electrochem. Soc.* **1991**, *138*, 3224. (b) Oppenheim, I. C.; Trevor, D. J.; Chidsey, C. E. D.; Trevor, P. L.; Sieradzki, K. *Science* **1991**, *254*, 687. (c) Chen, S. J.; Sanz, F.; Ogletree, D. F.; Hallmark, V. M.; Devine, T. M.; Salmeron, M. *Surf. Sci.* **1993**, *292*, 289.

(10) (a) Zhang, X. G.; Stimming, U. *Corros. Sci.* **1990**, *30*, 951. (b) Sanchez, M. P.; Barrera, M.; Gonzalez, S.; Souto, R. M.; Salvarezza, R. C.; Arvia, A. J. *Electrochim. Acta* **1990**, *35*, 1337.

(11) McCarley, R. L.; Bard, A. J. *J. Phys. Chem.* **1992**, *96*, 7410.

0002-7863/94/1516-10725$04.50/0

the dissolution of Cu in a variety of electrolytes, e.g., SO_4^{2-},[13] PO_4^{2-},[14] Cl^-,[15] and ClO_4^-,[10] have appeared. The current study is an effort to investigate the dissolution of Cu at the atomic level in the presence of aqueous Cl^-. The Cu/Cl^- system is particularly favorable for in situ STM, since Cl^- adsorbs strongly on Cu and the resulting surface remains oxide-free.[16]

Several electrochemical studies have been carried out to elucidate the mechanism of the dissolution of Cu at various Cl^- concentrations and at different pH values in aqueous solutions.[15] Two distinct regions can be discerned from current–potential curves for Cu in aqueous Cl^-: the apparent Tafel region and the limiting current region. Electrodissolution of Cu in the apparent Tafel region has been found to be either mass transfer or activation controlled. The proposed mechanism for dissolution is thought to follow the scheme given below for $[Cl^-] < 1$ M:[15]

$$Cu + Cl^- \rightarrow CuCl_{(ads)} + e \quad (1)$$

$$CuCl_{(ads)} + Cl^- \rightarrow CuCl_2^- \quad (2)$$

The initial step is the adsorption of Cl^- at the Cu surface followed by reaction 1 to form adsorbed CuCl. The rate of this reaction is potential dependent and therefore activation controlled. The rate of reaction 2, the desorption of the $CuCl_{(ads)}$ by reaction with additional Cl^- to form the soluble $CuCl_2^-$ complex, depends on the rate of diffusion of this complex away from the electrode surface. In the limiting current region, with $[Cl^-] < 1$ M, a porous film of CuCl is formed and the mass transport of Cl^- through the film is rate determining. A direct conversion of Cu^0 to Cu^{2+} also occurs in the limiting current region.[15] At higher Cl^- concentrations, i.e., $[Cl^-] > 1$ M, higher complexes, $CuCl_x^{(1-x)}$ (where $x = 2-4$), dominate and must be considered.

An in situ electrochemical STM investigation involves observation at high spatial resolution, preferably at the atomic level, of the evolution of surface structures with time. These observations require that the rate of change of the surface, controlled by the substrate current density and potential, be controlled on a time scale compatible with that of the STM image acquisition. This necessarily implies that the mechanistic information obtained in such studies applies over a limited range of current density and potential. Moreover, in STM experiments, one must be aware of the possibility of tip–substrate interactions. In this study, two are of particular concern. The potential applied to the tip can affect the potential on the substrate immediately below it, since the presence of tip tunneling current implies electrical contact between the tip and substrate in the usual sense. For example, a tip–substrate interaction has been previously observed for Pb electrodeposition on graphite,[8f] where it was found that variations in tip potential affected the deposition of Pb in the area being imaged. This interaction was attributed to an alteration of the potential distribution on the substrate by the close proximity of the biased tip (<1 nm). Deposition of Cu on the tip must also be avoided, because this would alter the tip area for tunneling and the tip–substrate distance. Such interactions were avoided by setting the tip potential above the Cu deposition potential and adjustment of the tip–substrate spacing (i.e., tunneling current). On the basis of the following observations, we did not find evidence of a tip-assisted etching process during dissolution experiments: (1) The type of etching observed here is inconsistent with what one would expect for tip-induced etching, i.e., pit formation. (2) No square pattern was found after scanning was confined to a small area (~10–20 nm on a side) for several minutes and then zoomed out to scan a much larger area (~100 nm on a side). (3) Tip–substrate interactions usually also show up as streaks in the image when the tip scans along the x-axis. This was not observed under the conditions of this study.

Experimental Section

Chemicals. High-purity water (Milli-Q purification system, >18 MΩ cm) was used throughout. Potassium chloride (J. T. Baker) and hydrochloric acid (Fischer) was used as received. All other chemicals were reagent grade or better.

Instrumentation. In situ images were obtained in ambient on a NanoScope III scanning tunneling microscope (Digital Instruments, Santa Barbara, CA) using the electrochemistry base and electrochemically etched W tips. The tips were 0.010-in. W rods (FHC, Inc., New Brunswick, ME) etched in 1 M KOH at 15 V ac. The etched tip was then rinsed with Millipore water followed by acetone. To reduce faradaic currents at the tip, the tips were insulated with either clear fingernail polish or polyethylene. The tip was coated with the polyethylene in a manner similar to that used to insulate tips with Apiezon wax.[17] The polyethylene produced an even coating and did not contaminate the solution in the cell as quickly as the nail polish. The contamination can be determined from degradation of the current–potential curve and the appearance of foreign matter on terraces over time. The electrochemical cell was fabricated from Kel-F with the Cu crystal serving as the base of the cell utilizing either a Viton or Teflon O-ring to complete the seal. A AgCl-coated Ag wire served as the reference electrode and a Pt wire as the counterelectrode. However, all potentials, including the tip bias (V_{tip}), are given with respect to a saturated calomel electrode (SCE). All images were taken in the height mode, i.e., at constant current, unless otherwise noted, with observations made on consecutive days under similar conditions. All of the images presented represent raw data and are unfiltered.

Substrate. Cu(111) single crystal disks (1-in. diameter) (a gift from Dr. Thomas Moffat, NIST) were cut into square pieces (0.9 cm × 0.9 cm) after the substrate orientation was determined by Laue X-ray back-reflection. The crystal was placed in the electrochemical cell with a known orientation of the substrate lattice with respect to the STM x- and y-scan directions. Surface preparation involved mechanical polishing down to 0.25-μm diamond paste followed by electropolishing in a 1:1 (by volume) water/orthophosphoric acid bath at ~0.2 A/cm² for approximately 3–5 min.[18] This procedure resulted in a consistent mirrorlike finish. The crystal was then rinsed with Millipore water. A drop of water was left on the surface to protect it during transfer to the STM cell. Because of the cell configuration and experimental considerations, the solutions used in this study were not deaerated nor was oxygen excluded from the cell surroundings. This was not a problem, since the Cu etching rate could be controlled by adjustment of the electrode potential as discussed below.

Results and Discussion

STM Imaging of Adsorbed Chloride. Imaging a freshly polished surface at open circuit in 10 mM HCl proved to be difficult due to the presence of oxide surface structures formed during the electropolishing step. To clean the surface of the oxide, the freshly electropolished surface was immersed in 10 mM HCl at the rest potential, −0.035 V vs SCE, and the potential was swept negative at 20 mV/s to the hydrogen evolution region, then back into the Cu dissolution region, and

(12) Bertocci, U.; Turner, D. R. In *Encyclopedia of Electrochemistry of the Elements*; Bard, A. J., Ed.; Marcel Dekker: New York, 1974; Vol. II, Chapter II-6.

(13) Fonseca, I.; Marin, A.; Sa, A. *Electrochim. Acta* **1992**, *37*, 2541.

(14) Pointu, B.; Braizaz, M.; Poncet, P.; Rousseau, J. *J. Electroanal. Chem.* **1981**, *122*, 111.

(15) (a) Barcia, O.; Mattos, O.; Pebere, N.; Tribollet, B. *J. Electrochem. Soc.* **1993**, *140*, 2825. (b) Cooper, R. S.; Bartlett, J. H. *J. Electrochem. Soc.* **1958**, *105*, 109. (c) Lee, H. P.; Nobe, K. *J. Electrochem. Soc.* **1986**, *130*, 403. (d) Braun, M.; Nobe, K. *J. Electrochem. Soc.* **1986**, *126*, 1666.

(16) Stickney, J. L.; Ehlers, C. B. *J. Vac. Sci. Technol., A* **1989**, *7*, 1801.

(17) Nagahara, L. A.; Thundat, T.; Lindsay, S. M. *Rev. Sci. Instrum.* **1989**, *60*, 3128.

(18) Richardson, J. H. *Optical Microscopy for the Material Sciences*; Marcel Dekker: New York, 1971; p 460.

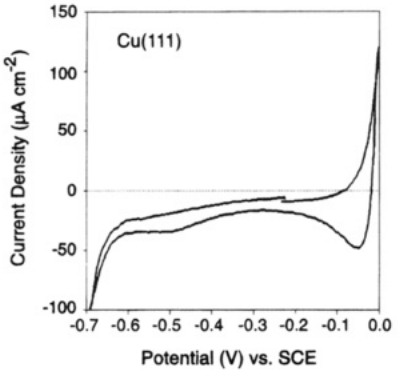

Figure 1. Current−potential curve for Cu(111) in 10 mM HCl in air after three complete potential cycles (scan rate 20 mV/s).

then finally to about −0.215 V in the double-layer region, where there should be no Cu dissolution and no surface oxide formation. Figure 1 shows a representative current−potential curve for the Cu(111) surface in 10 mM HCl at 20 mV/s after such a treatment. This current−potential curve agrees with previously reported curves obtained from clean, well-ordered Cu(111) surfaces in 10 mM HCl.[16] The small broad cathodic peak at ∼−0.5 V is probably associated with oxygen reduction,[19] since in voltammetric experiments with a Cu(111) electrode, the peak height decreased with increasing levels of degassing with Ar. An STM image obtained at −0.215 V after the dissolution and redeposition of Cu during the cyclic voltammetry (CV) did not disorder the surface as shown in Figure 2A. A well-defined terrace structure is present on the surface with terrace widths of 10−20 nm. The step heights, 0.20 ± 0.02 nm, are consistent with steps being one Cu atom in height, i.e., 0.18 nm.[20] Although images like this were easily obtained, the very large terraces seen here toward the middle of the image were not always present from day to day.

A zoomed view of the atomic structure of the Cl^- adlayer located on the large terrace in the center of Figure 2A (Figure 2B) shows a hexagonal lattice of atoms with nearest-neighbor distances of 0.39 ± 0.2 nm. The image skews somewhat in one direction because of thermal drift. The chloride adlattice is rotated 30° relative to Cu(111) substrate rows. The rotation and the distances of the adlattice are consistent with the $(6\sqrt{3}\times6\sqrt{3})R30°$ structure with a coverage of 0.45 (where coverage represents the number of adsorbate atoms per number of substrate surface atoms) proposed by Goddard and Lambert[21] from the low-energy electron diffraction (LEED) pattern following dosing with Cl_2 on Cu(111) in ultrahigh vacuum (UHV) and recently confirmed by an UHV-STM study of Cu(111) dosed with Cl_2.[22] The $(6\sqrt{3}\times6\sqrt{3})R30°$ structure has seven Cl atoms along the $6\sqrt{3}$ or {211} direction, which gives a Cl−Cl distance of 0.379 nm, in reasonable agreement with our measured distance of 0.39 ± 0.2 nm. This structure can be thought of as a compression structure where the Cl atoms pack closer as the coverage increases. Cu(111) electrodes emersed from millimolar HCl solutions have exhibited a LEED pattern termed the split $\sqrt{3}$. This LEED pattern is quite similar to the

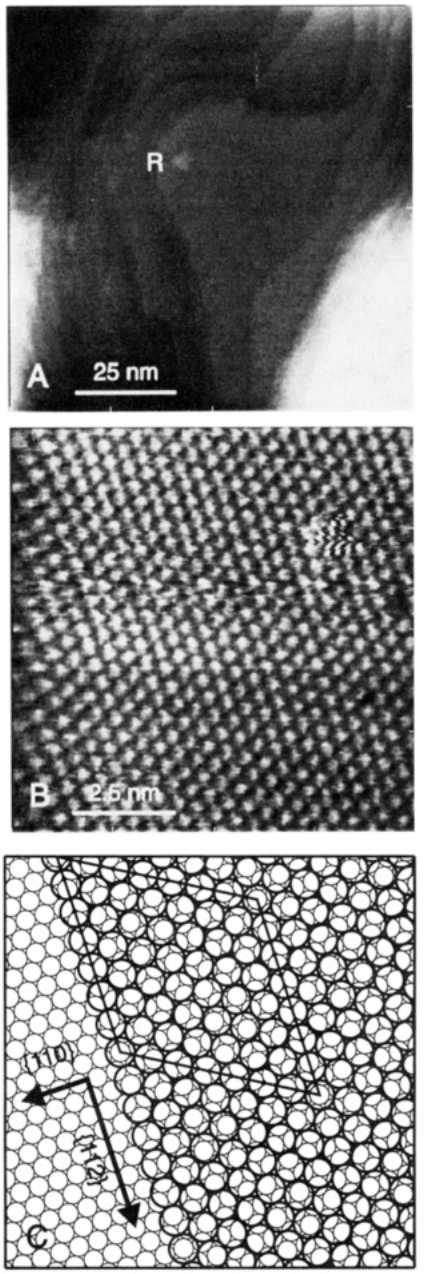

Figure 2. STM micrographs: (a) 100-nm image obtained at −0.215 V taken soon after the potential cycle shown in Figure 1 (V_{tip} = +21 mV and i_T = 3.0 nA), (B) 10-nm zoomed image taken on the large terrace shown in (A) at −0.215 V (V_{tip} = −200 mV and i_T = 9.0 nA), (C) depiction of the Cl compression structure on Cu(111). The larger wide-lined circles are Cl and the smaller thinner lined circles are Cu atoms. The outlined unit cell corresponds to the $(6\sqrt{3}\times6\sqrt{3})R30°$ structure. The structure as drawn is aligned with the STM picture in (B). All STM pictures presented here are oriented in a similar manner.

$(6\sqrt{3}\times6\sqrt{3})R30°$ observed by Goddard and Lambert and is consistent with the atomic image in Figure 2B. Thus, the structure observed in Figure 2B is composed of a hexagonal array of close-packed Cl atoms which forms an incommensurate structure with the Cu(111) substrate with a $(6\sqrt{3}\times6\sqrt{3})R30°$ unit cell as shown in Figure 2C. No other surface structure was observed over a potential range of −0.1 to −0.6 V vs SCE. However, the chloride could be desorbed by setting the potential into the hydrogen evolution region (potentials ≤−0.620 V). Desorption of Cl at these potentials has been proposed from Auger electron analysis of Cu(111) surfaces emersed from millimolar HCl solutions.[23] The Cu(111) substrate atoms have

(19) SECM experiments using a Cu substrate and a 5-μm-diameter Pt tip were performed to ascertain the nature of the cathodic peak in Figure 1. The tip potential was held at ∼−0.6 V, where oxygen reduction occurs, with a tip−substrate separation of ∼5 μm. The potential of the Cu substrate was stepped from −0.3 to −0.6 V (past the peak), and the tip and substrate currents were monitored. Upon stepping the substrate potential, the tip current decreased markedly due to oxygen reduction at the Cu substrate.

(20) *CRC Handbook of Chemistry and Physics*; Weast, R. C., Ed.; CRC Press: Boca Raton, FL, 1986.

(21) Goddard, P. J.; Lambert, R. M. *Surf. Sci.* **1977**, *67*, 180.

(22) Motai, K.; Hashizume, T.; Lu, H.; Jeon, D.; Sakurai, T. *Appl. Surf. Sci.* **1993**, *67*, 246.

(23) Ehlers, C. B.; Villegas, I.; Stickney, J. L. *J. Electroanal. Chem.* **1990**, *248*, 403.

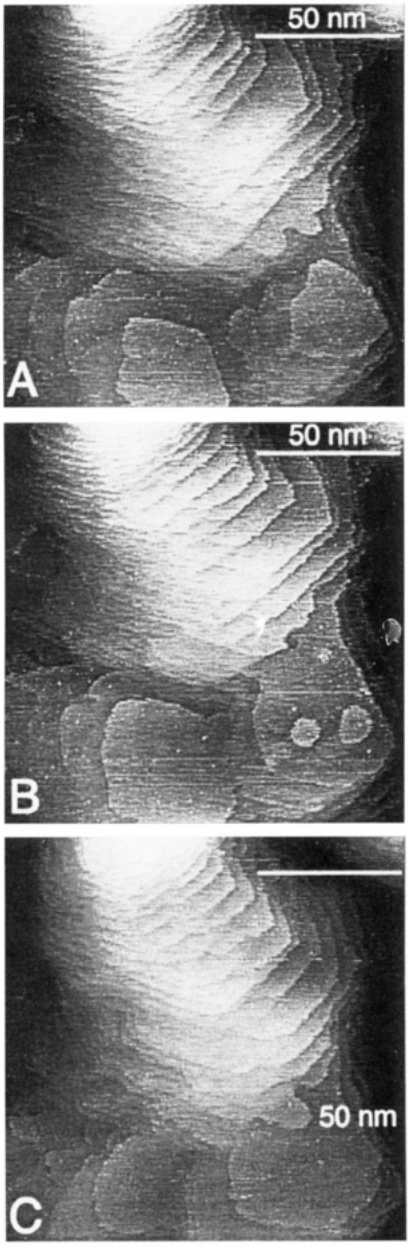

Figure 3. STM micrographs depicting the surface reordering process observed at −0.215 V with $V_{tip} = 10$ mV and $i_T = 8.7$ nA (time between images 50 s). These images have been contrast-enhanced to make the terrace edges clearer.

been observed by in situ AFM in 0.1 M $HClO_4$ at potentials within the double layer.[24]

Surface Reordering. Continuous imaging of the Cu(111) surface at a potential of −0.215 V vs SCE, about 0.2 V negative of where Cu dissolution starts (i.e., $E < E_d$ where E_d is the starting potential for Cu dissolution), resulted in changes in surface morphology (reordering). These changes can be seen in the sequence of images in Figure 3. A series of Cu(111) terraces of varying length run almost diagonally from a high point in the upper left-hand corner to a series of large terraces in the lower portion of the images. These terraces are dynamic, and their widths change continuously. The higher shorter terraces slowly grow wider while the lower terraces become smaller. Another smaller hill in the lower right-hand portion of Figure 3A shows similar behavior; i.e., the upper terrace decreases, and the lower terrace increases. In Figure 3B, the lower terrace in the series of terraces has merged with the second lowest terrace from the lower hill in Figure 3A to form one complete terrace. These trends continue with Figure 3C.

Analogous reordering has been observed by LEED for Cu(100) single surfaces exposed to ion bombardment and mechanical polishing after immersion in HCl solution.[25] This reordering is probably the result of diffusion of Cu atoms at step edges, especially where two step edges meet. The terraces in the upper portion of the images in Figure 3 have such connections on both the left and right sides. The rapid diffusion of the Cu atoms is probably the result of the adsorbed Cl, which weakens the bonds between the topmost Cu layer and bulk Cu, especially at kink sites, resulting in a lower barrier for diffusion. Similar Cl^--enhanced mobility has been observed for Au(111) surfaces after oxide formation and reduction in 0.1 M $HClO_4$ and 0.1 M $HClO_4/1 \times 10^{-5}$ M Cl.[26] Some of the morphology changes did not have direct connection to a step edge, however. For example, the two islands on the lower terrace in Figure 3B disappear in Figure 3C, and the lower terrace is somewhat larger. Ag(111) smoothes out with time after applying oxidation−reduction cycles.[27] This is attributed to the dissolution of Ag atoms residing at unfavorable sites to form Ag complexes which then redeposit at more favorable sites. This mechanism leads to the disappearance of large features in a single scan and could account for the disappearance of the large islands in Figure 3B.

We cannot totally rule out the possibility of tip−substrate interaction causing some surface changes. However, imaging at lower tunneling currents (larger tip−substrate separation) did not affect the observed changes in step edges.

Anodic Dissolution of Cu(111) (HCl). When the potential of the Cu(111) surface is swept slowly (1−2 mV/s) positive in 10 mM HCl (pH 2.1) to potentials >−0.08 V vs SCE, dissolution of Cu begins. Potentials were selected where the rate of Cu dissolution was low, and therefore successive STM images showed obvious, but not too drastic, differences. This was accomplished by sweeping the potential positive from −0.215 V at 1−2 mV/s. Images were taken away every 30 s, and when the imaging showed signs of moderate dissolution, the potential sweep was stopped. The resulting substrate current was usually 0.5−1 μA (0.65−1.3 μA cm^{-2}). To maintain stable imaging, the tip was held at +21 mV, a value positive of the rest potential (−0.215 V), so that Cu would not deposit on the tip and alter its morphology. The bias between the tip and substrate, $V_{substrate} - V_{tip}$, was kept small to minimize any effect of the tip potential on the potential of the substrate immediately below the tip.

Figure 4 represents a series of STM images taken at various times during the dissolution experiment described above. Figure 4A was taken at −0.03 V after scanning the potential from the condition of Figure 2A (−0.215 V) at 2 mV/s. A small thermal drift occurred during acquisition of the zoomed images in Figure 4; a high reference mark, R (probably a surface impurity), is shown in each image and in Figure 2A to provide a common reference point. Terraces of interest (T1, T2, T3) in the images are marked to show progressive changes in each terrace with time. In the lower right-hand corner of Figure 4, a compass of the orientation of the underlying Cu substrate in all of the images is shown. A total of 60 images were acquired during this sequence; those in Figure 4 are representative of the results at various times and show the general trends observed during dissolution. The rate of dissolution at −0.03 V is quite slow, as shown by the small changes between parts A and B of Figure

(24) Cruickshank, B. J.; Sneddon, D. D.; Gewirth, A. A. *Surf. Sci. Lett.* **1993**, *281*, L308.

(25) Villegas, I.; Ehlers, C. B.; Stickney, J. L. *J. Electrochem. Soc.* **1990**, *137*, 3143.

(26) Trevor, D. J.; Chidsey, C. E. D. *J. Vac. Sci. Technol., B* **1991**, *9*, 964.

(27) Aloisi, G.; Funtikov, A. M.; Guidelli, R. *Surf. Sci.* **1993**, *293*, 291.

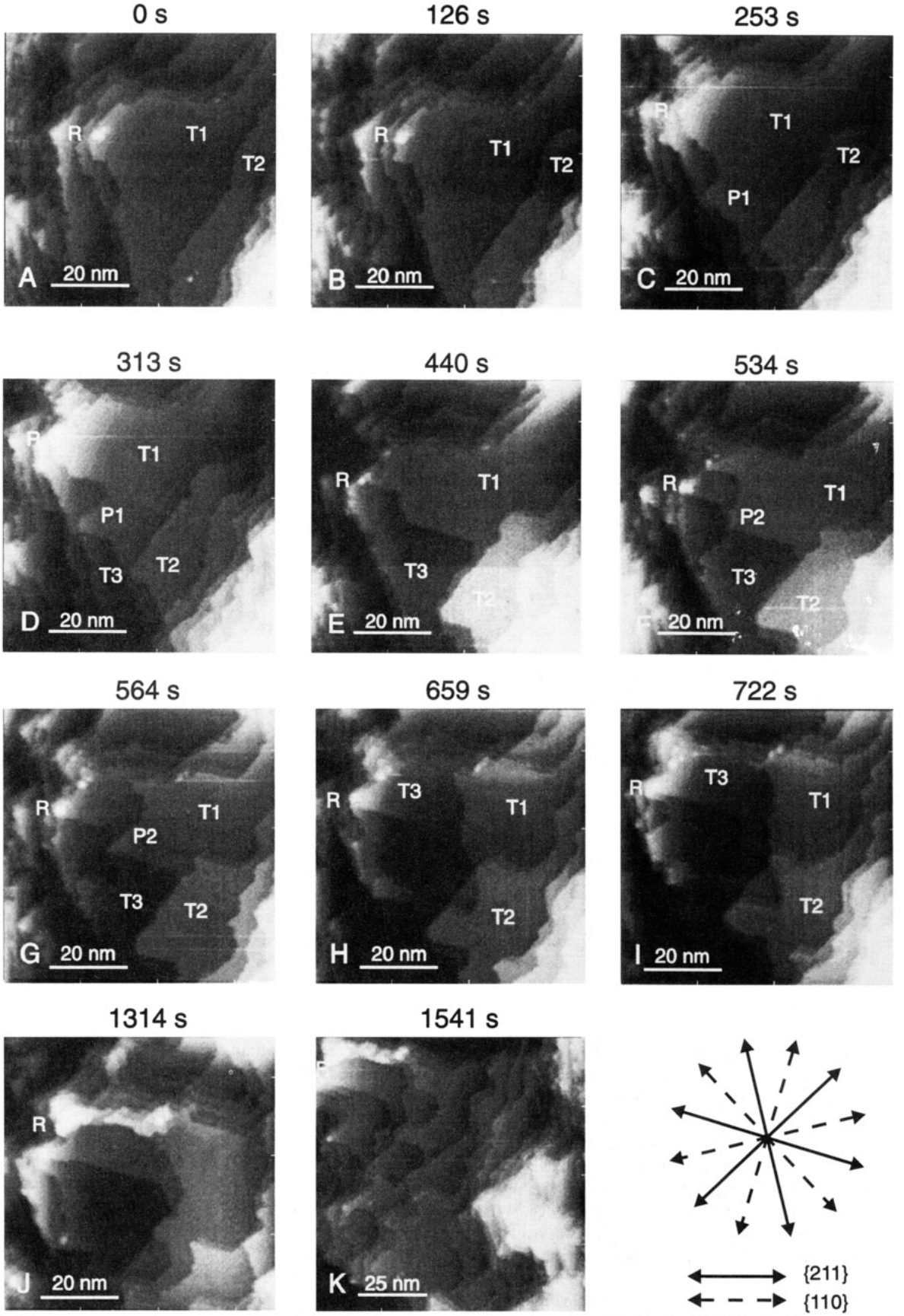

Figure 4. STM micrographs taken over a period of time showing the anodic dissolution of Cu(111) in 10 mM HCl: (A) 70-nm image taken after scanning the potential from −0.215 to −0.03 V at 2 mV/s (V_{tip} = +21 mV and i_T = 9.0 nA), (B) 70-nm image at the same potential as (A) 126 s later, (C) 70-nm image taken after scanning the potential from −0.03 to 0 V at 2 mV/s (V_{tip} = 21 mV and i_T = 9.0 nA), (D−J) 70-nm images taken at various time intervals at 0 V (V_{tip} = 21 mV and i_T = 9.0 nA), (K) 100-nm image taken at the final time of 1541 s at 0 V (V_{tip} = 21 mV and i_T = 9.0 nA). Times between scans are noted above each image, and a reference point R is marked on all images to give a common position. The lower right-hand corner indicates the orientation of the Cu(111) substrate and shows {211} (solid lines) and {110} (dashed lines) directions.

4. There was no evidence of pitting at this potential, but some step edges on the surface appeared to lose a small amount of material (see T1 and T2). To increase the rate of dissolution, the substrate potential was swept to 0 V (in ~15 s, with V_{tip}

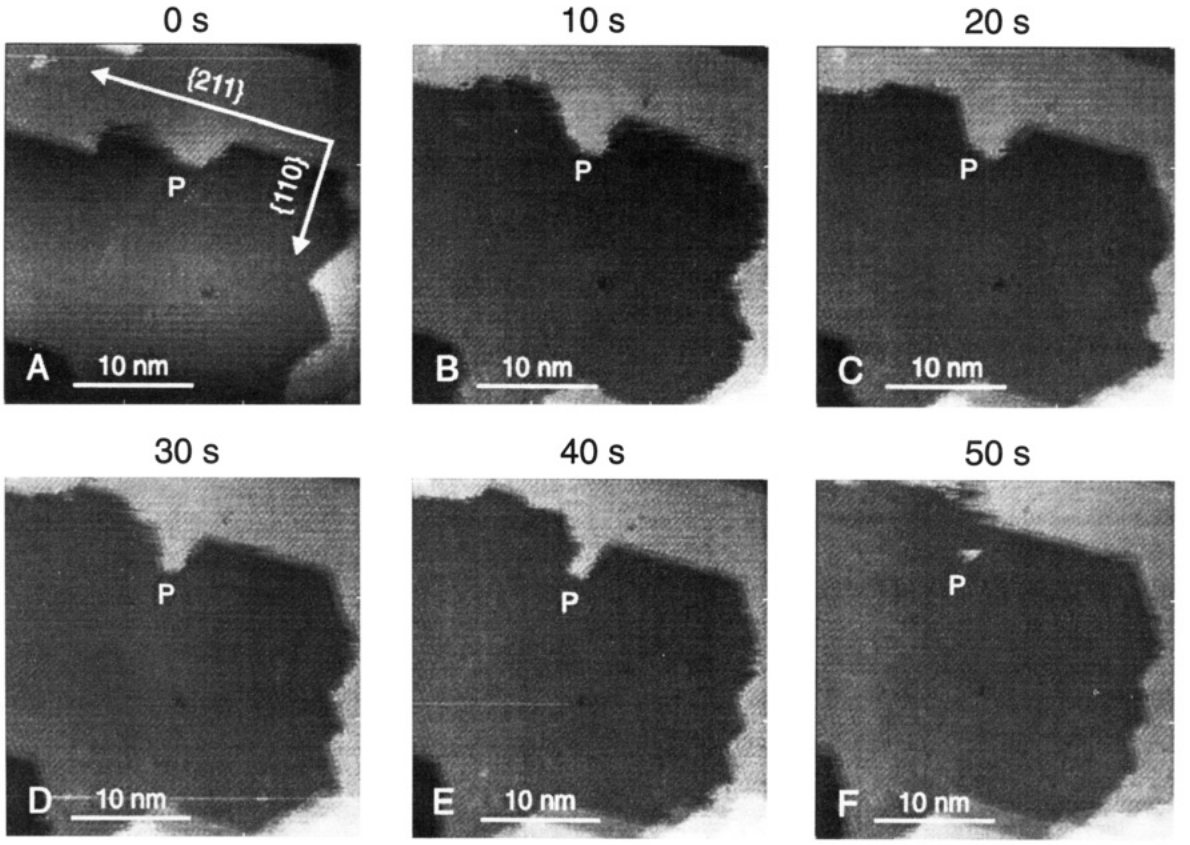

Figure 5. STM micrographs showing the formation of a facet, F, along a dissolving {211} step at various time intervals which are given above each image (potential 0 V, $V_{tip} = 21$ mV, and $i_T = 9.0$ nA). Notice that the apex of the facet is pinned and dissolution occurs around the pinned point until new edges attack the sides and finally dissolve the whole facet.

held at 21 mV); Figure 4C, acquired just after completion of this sweep, shows that the rate of dissolution has increased compared to that in Figure 4A,B and that the initial stages of Cu dissolution are potential dependent and activation controlled. Comparing parts B and C of Figure 4, we see that the dissolution has continued, and that the edges along the {211} direction are the primary dissolution points. The edges do not retreat evenly but, rather, leave protruding points or peninsulas. This type of behavior was observed throughout the dissolution experiment and is discussed in detail below. In Figure 4C, for example, we see the development of a triangular peninsula, P1, on T1; this is well developed in Figure 4D. In Figure 4E, the entire peninsula and a large portion of the terrace below have dissolved. In Figure 4F, another peninsula, P2, develops on T1 and has a similar fate. The uneven retreat of the edges causes the formation of roughly hexagonal indentations in the terrace as the dissolution proceeds (see, for example, Figure 4K). Upon closer inspection of the images, one can account for this by pinning of the outer edge of the pit (discussed below), with dissolution of the step continuing to form a triangular facet. Edges can be pinned over long distances, i.e., 10−25 nm, with dissolution halted or slowed dramatically along the edge. When distant points on the terrace edge become pinned, hexagonal-shaped indentations develop. The interior edges are created from the preferential dissolution of the step edge in the {211} direction. This pinning effect is better illustrated in Figure 5A−D. In the first image, a peninsula, P, begins to form. As the edge retreats around the pinned apex, the peninsula becomes more pronounced, forming a well-defined triangular peninsula. As pointed out above, we rarely observe step edges in the {110} direction, but in Figure 5A, we see a 2−3-nm {110} step edge. However, in the images that follow, this edge retreated quickly to form a {211} step edge. The dissolution rate around the peninsula decreased relative to the advance of the step edge in the rear. But as the edge continued to retreat, the peninsula edges became exposed and finally dissolved, leaving a remnant at the apex, Figure 5F. This type of behavior is probably caused by the presence of an impurity atom (e.g., of a more noble metal) in the Cu lattice. Sulfur is also a common impurity in Cu and, at these potentials, would be resistant to dissolution, effectively pinning an edge. This general type of behavior has been treated theoretically by Chui and Weeks,[28] who have shown that step edges can be pinned by impurity points over relatively long distances.

The lower portion of terrace T1 in Figure 4D is also of interest. Dissolution of the edge of T1 toward the top of the image continued unabated along a {211} edge pinned at the apex of P2, but dissolution of the edge toward the lower right-hand corner slowed dramatically when it reached the overlying terrace T2 (see the sequence of images in Figure 4D-G). The slow dissolution of the lower terrace, T1, was probably caused by a lack of movement of the upper terrace. When the two come together, they create a two-atom-high step which is harder to etch, therefore pinning the two in place. Note that terrace T2 holds an essentially constant shape from part E to part G of Figure 4, and the lower left-hand corner of this terrace seemed to be pinned as noted with both P1 and P2 described above in Figure 4. In Figure 4I, however, terrace T2 etches along the {211} edge, and in subsequent images (not shown here), the underlying terrace T1 begins to dissolve as terrace T2 retreats further back. The reference point R also acts as a pinning point, since {211} edges stop dissolving as they approach R. Figure 4J shows the surface after 17 min of dissolution at the same potential, and Figure 4K represents a 100-nm view of the same area (see reference mark R for comparison with the rest of Figure 4). Note that in the ~10 min between parts I and J of

(28) Chui, S. T.; Weeks, J. D. *Phys. Rev. B* **1981**, *23*, 2438.
(29) Perkins, L. S.; Depristo, A. E. *Surf. Sci.* **1993**, *294*, 67.

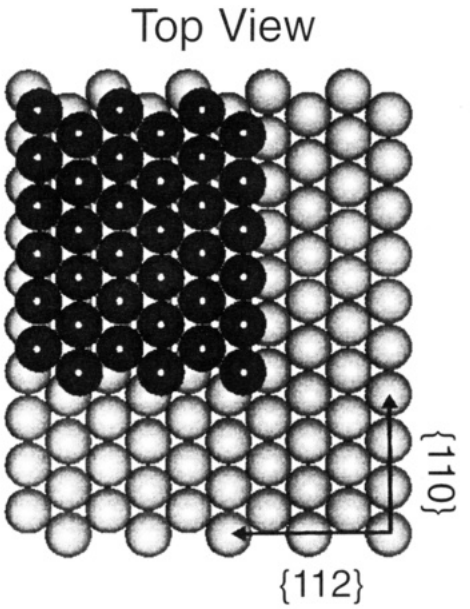

Figure 6. 3D views of a step edge on Cu(111) illustrating the difference in geometry between steps in the {110} and {211} directions. The darker atoms are the top layer, and the lighter atoms are the bottom layer. The high density of kink sites in the {211} direction is quite clear.

Figure 4 atomic imaging was performed on a 10−20-nm scale (see Figure 5). After zooming back out to the larger 100-nm image (Figure 4J), there was no evidence for tip-induced alterations during the high-resolution scans with smaller tip−substrate distances. Tip−substrate interactions usually produce a clear square pattern when scanning a large area immediately after high-resolution imaging.

Dissolution from step edges is energetically favorable compared to removal of a Cu atom at the center of a (111) terrace, because of the higher coordination per Cu atom in a terrace relative to an atom at a step edge.[29] This also leads to the surface reordering discussed in the previous section. Steps running along the {211} direction are the preferred edges for dissolution (Figure 4). This is the $\sqrt{3}$ direction on Cu(111), i.e., rotated 30° relative to the (111) substrate rows. The Cl atoms run along these rows, but the underlying Cu atoms along this direction are in a configuration where there are kink sites at every position along the edge. This is illustrated in Figure 6, which displays two view of a Cu(111) surface with a second Cu layer cut away to show the ideal atomic arrangement for step edges in the {211} and {110} directions. The Cu atoms on the step edges in the {211} direction are energetically easier to remove than those in steps along {110} rows,[30] where the Cu atoms lie side by side with higher coordination (i.e., a Cu atom within a {110} row coordinates with four Cu atoms in the same plane, while one within a {211} row coordinates with three). Therefore, the {211} edges are preferentially etched, because the high number of kink sites provides attractive dissolution sites relative to the {110} step edge. Dissolution along other step edges (as seen from atomic scale images) has also been observed, i.e., along the {110} direction (see Figure 5A,B), but these edges tend to be small (length 2−3 nm) and quickly dissolve to form a step edge in the {211} direction, perhaps through initial removal of Cu atoms at the corners (i.e., at the intersection of two edges), which have an even smaller in-plane coordination. We therefore propose that the initial stage of dissolution involes a Cl^- ion reacting with a Cu atom at a kink site, forming a CuCl species as in reaction 1, with dissolution of the CuCl from the edge to form the $CuCl_2^-$

(30) Liu, C. L.; Adams, J. B. *Surf. Sci.* **1993**, *294*, 211.

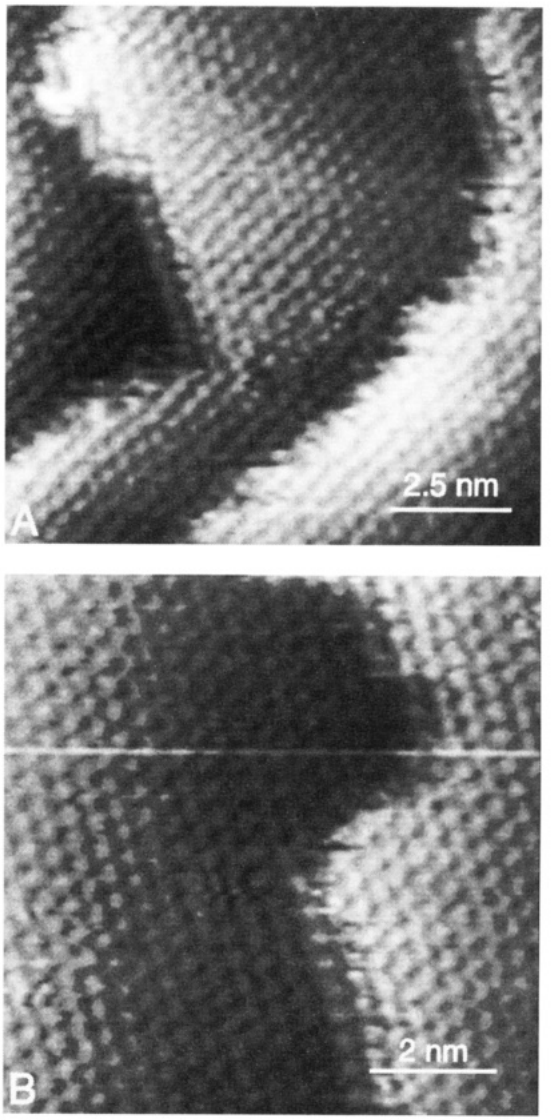

Figure 7. Atomic images of various step edges taken at −0.03 V (V_{tip} = +21 mV, 9.0 nA). These images, taken between the images in Figure 4I,J while dissolution was occurring, show Cl adsorbed at edge sites.

species. After reaction 2, another Cl^- atom diffuses in to replace the Cl atom desorbed from the surface in reaction 2. We have never observed bare copper at the dissolving edges. This is illustrated by the images in Figure 7, where several atomically resolved steps are shown. We should note that these images were taken during the time that elapsed between the images in Figure 4I, J, where Cu dissolution was occurring. The frizziness of the steps running diagonally in Figure 7A suggests that the Cu atoms are in motion, i.e., dissolving along the {110} direction. Some steps show Cl atoms at an intermediate height between the two terraces, and this is shown well in the almost vertical {110} steps in Figure 7. These images revealed no Cu atoms at these steps. The intermediate Cl atoms probably represent adsorbed Cl atoms at a kinked edge, which act as dissolution points for reaction 2.

The energetic differences alluded to above suggest that microscopic potentials for different Cu sites are different. For example, one can write formally

$$Cu(I)_{soln} + e \rightleftarrows Cu_{terr} \qquad E^\circ_{terr}$$

$$Cu(I)_{soln} + e \rightleftarrows Cu_{edge} \qquad E^\circ_{edge}$$

where $Cu(I)_{soln}$ represents dissolved Cu(I) species (e.g., $CuCl_2^-$) and Cu_{terr} and Cu_{edge} represent the assembly of those atoms in

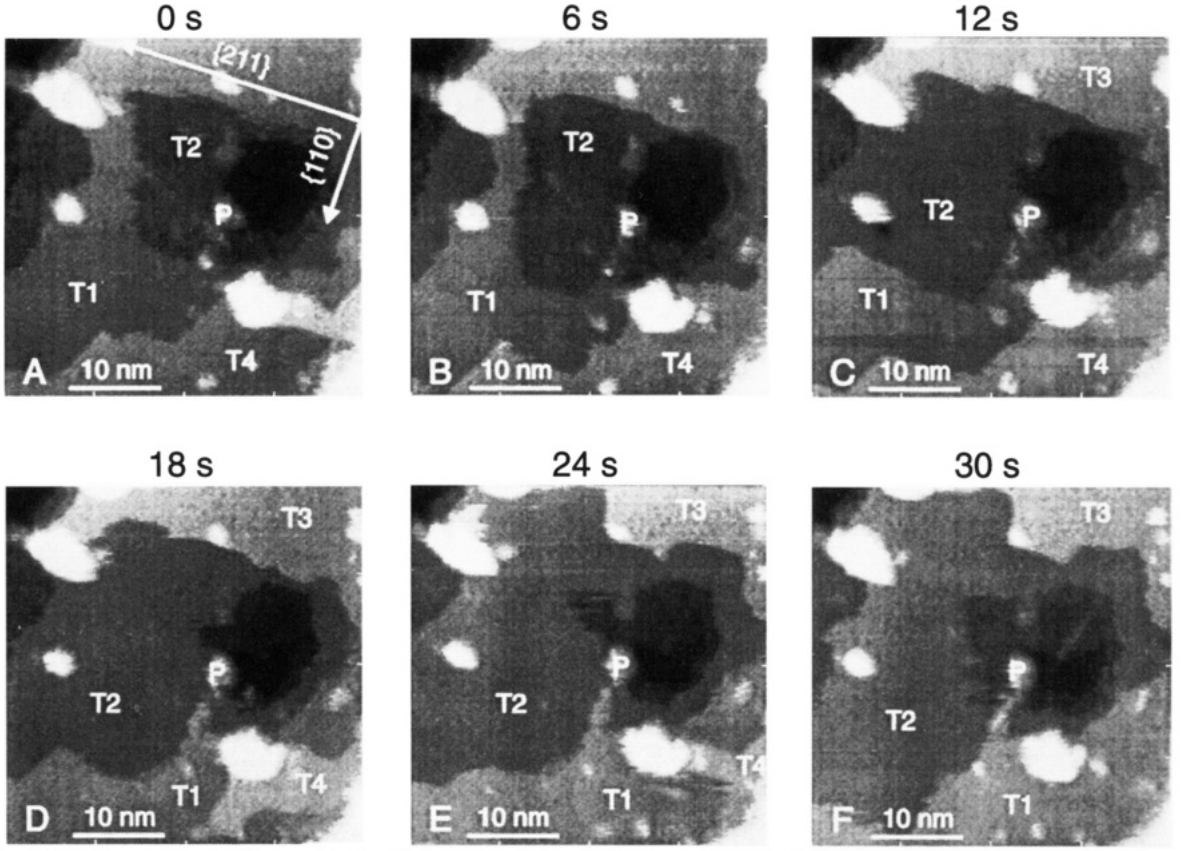

Figure 8. STM micrographs showing anodic dissolution of Cu in 10 mM KCl at −0.03 V with V_{tip} = 50 mV and i_T = 7.0 nA. The protrusion P just to the left of the pit is the most reactive site on this surface, and step edges are seen to dissolve away from the pit while new step edges form inside the pit. Several pinning points are found in these pictures, and they are discussed in the text. The rate of dissolution in these images is also faster than that found in Figure 4.

terraces and step edge sites. Energetic considerations suggest that $E^\circ_{terr} > E^\circ_{edge}$, so the free energy for the reaction

$$Cu_{edge} \rightleftarrows Cu_{terr} \qquad E^\circ_{terr} - E^\circ_{edge}$$

is negative, i.e., favoring loss of edges and growth of terraces, as observed during reordering. Indeed, an even more detailed energetic model might be proposed, e.g., for different edge orientations (for example, $E^\circ_{edge\{110\}} > E^\circ_{edge\{211\}}$). However, in the absence of a method of determining surface energetics for different sites, the magnitudes of the local E° values cannot be determined. A theoretical approach relating these differences to the extent of coordination to the Cu atom (i.e., as coordination increases, E° becomes more positive) is a possibility. These ideas imply that the standard E° value for a solid metal represents an averaging over different sites and, in practice, over different crystal faces. This conclusion can clearly be drawn from extensive past work which has shown that low-index planes of metal surfaces show different reactivity and different work functions. We suggest here that this concept can be extended to different sites on the (111) plane.

When the potential of the Cu(111) electrode was made even more positive, the rate of dissolution accelerated and imaging of the surface became more difficult than at the potentials used in Figures 4 and 5. The images reveal that the dissolution still occurs at step edges, but preferential etching in one direction is not observed; i.e., all step edges were vulnerable to dissolution. Studies of the dissolution in the limiting current region are continuing and will be presented in a subsequent paper.

We have also carried out studies of anodic dissolution of the Cu(111) surface in 1 mM HCl. The results are qualitatively similar to those presented for 10 mM HCl, with dissolution occuring preferentially at {211} step edges. The same atomic structure was also observed with 1 mM HCl as that discussed above for 10 mM HCl (Figure 2B).

Anodic Dissolution of Cu(111) (KCl). Studies of Cu dissolution in KCl solutions at pH 6.5 were qualitatively the same for 1 and 10 mM KCl. As with 10 mM HCl, the electrode was cycled several times to obtain a steady-state cyclic voltammogram. A regular terrace structure was observed in KCl with 10−20-nm terrace widths. Very large terraces, as seen with 10 mM HCl, were generally not observed. As with 10 mM HCl, terrace edges were found to run along the {211} direction. Atomic imaging of the surface revealed the same structure as that observed for 10 mM HCl shown in Figure 2B. One interesting difference between KCl and HCl was the presence in KCl of many point defects in the Cl adlattice. Similar defects were only observed at higher dissolution potentials with HCl. The number of point defects increased as the potential approached E_d. The presence of these pits could be attributed to impurities from solution or to the presence of oxygen in the Cl adlattice. The presence of oxide structures would not be totally unexpected in the KCl solution at pH 6.5, since copper oxides could form and are stable at this pH.[12]

As with 10 mM HCl, a slow sweep (1−2 mV/s) was made from −0.215 V to where the Cu dissolution process occurred at a moderate rate (−0.03 V). Figure 8A−D is representative of the dissolution behavior observed in this medium. Again, we have labeled key terraces. A pit several atoms deep appears on the right side of all of the images. The edges of the pit slowly dissolve from right to left through the sequences of images. Although it is difficult to see in these images, there is a smaller pit inside the larger one right near the white protrusion, P. In about 50 images of dissolution in this area, pits always began just to the right of P and dissolved to the right. This site seems to be a reactive one, perhaps a dislocation or other surface

defect. Preferential dissolution at such sites has been observed previously for other metals.[5] The other protrusions in the images, i.e., the white circular areas, are not reaction centers like P, since dissolution around them occurs only via the step edge mechanism. However, these sites do hinder the dissolution.

As for 10 mM HCl (Figure 4), the primary edges for dissolution were in the {211} direction. Some pinning was also noticed in these images. This is illustrated by the large terrace T3 shown in Figure 8D–F. In Figure 8D, the edge of T3 is relatively straight and retreated upward at a fairly constant rate. In Figure 8D, the terrace edge of T3 contacted a small protrusion (white spot), and the images that follow reveal that the step edge became pinned at this site. The edge continued to dissolve around the protrusion, developing a second {211} edge 60° from the advancing edge. Both to the left and to the right of this protrusion another point has been pinned, creating a hexagonal-shaped step edge. Several of these protrusions can be seen in Figure 8, and similar behavior is found for all of them. The protrusions seen in Figure 8 are probably impurities (sulfur, organics, oxides) on the Cu surface. These impurities would effectively block the surface Cu atoms underneath them (e.g., from Cl^- attack), making them more resistant to dissolution. However, the high reactivity near protrusion P probably indicates a surface defect of a different kind that provides a catalytic site.

The rate of dissolution in KCl is faster than with 10 mM HCl (note the different time scales in Figures 4 and 8, at the same potential). The frizziness on some of the step edges in Figure 8 also suggests the step edges are undergoing more rapid dissolution during imaging. Previous studies have also shown that higher concentrations of K^+ relative to H^+ at constant pH result in higher diffusion currents and hence a faster rate of dissolution.[14] This was attributed to an increase in the transference number for Cl^- in KCl vs HCl.

Conclusions

In situ STM analysis has been used to examine the anodic dissolution of Cu(111) in aqueous Cl^- solutions with atomic resolution. Cl was found to adsorb in a hexagonal compression structure rotated 30° relative to the Cu substrate rows at a coverage of 0.45 across the entire Cu(111) surface. This structure had been previously observed by LEED and UHV-STM. Cu dissolution proceeded via step edges at moderate dissolution potentials in both HCl and KCl at concentrations of 1 and 10 mM. The step edges along the {211} directions were found to preferentially dissolve, probably due to the high concentration of kink sites along the underlying Cu edge. Dissolution resulted in an uneven retreat of the step edges probably because of the presence of impurities in the lattice, e.g., S or lattice defects, that can pin an edge. The rate of dissolution was faster in the presence of K^+ vs H^+, as seen in earlier studies of the mechanism of Cu dissolution in Cl^-. Dissolution at higher potentials showed that a step edge mechanism was still favored, but the process was more random and did not necessarily follow a given step direction.

Acknowledgment. The authors gratefully acknowledge the support of the Office of Naval Research and the Robert A. Welch Foundation. We would also like to thank Shueh-Lin Yau for helpful discussions, Dr. Steve Swinnea for helping with the Laue back-reflection equipment, and Dr. Tom Moffat for supplying the Cu single crystals.